From Molecules to Frameworks: Variable Dimensionality in the $UO_2(CH_3COO)_2 \cdot 2H_2O/HF_{(aq)}$/Piperazine System. Syntheses, Structures, and Characterization of Zero-Dimensional $(C_4N_2H_{12})UO_2F_4 \cdot 3H_2O$, One-Dimensional $(C_4N_2H_{12})_2U_2F_{12} \cdot H_2O$, Two-Dimensional $(C_4N_2H_{12})_2(U_2O_4F_5)_4 \cdot 11H_2O$, and Three-Dimensional $(C_4N_2H_{12})U_2O_4F_6$

Susan M. Walker, P. Shiv Halasyamani,† Simon Allen, and Dermot O'Hare*

Contribution from the Inorganic Chemistry Laboratory, University of Oxford, South Parks Road, Oxford, U.K. OX1 3QR

Received June 23, 1999

Abstract: The hydrothermal syntheses and structures of a new series of organically templated uranium materials are presented. The materials are found in the $UO_2(CH_3COO)_2 \cdot 2H_2O/HF_{(aq)}$/piperazine system and span the range of dimensionalities from molecular, zero-dimensional, $(C_4N_2H_{12})UO_2F_4 \cdot 3H_2O$ (UFO-8a and -8b) through framework, three-dimensional, $(C_4N_2H_{12})U_2O_4F_6$ (MUF-1). It is stressed that this multidimensional series is synthesized by utilizing the *same template molecule*. Stability regions, wherein pure phases are synthesized, have been determined and depicted graphically through composition space and prism diagrams. The diagrams have allowed us to rationalize the product formed on the basis of initial reagent concentrations. The reported materials have been characterized by single-crystal X-ray diffraction, thermogravimetric analysis, and infrared and Raman spectroscopy. The zero-dimensional, or molecular, phases, $(C_4N_2H_{12})UO_2F_4 \cdot 3H_2O$ (UFO-8a and -8b), contain dimers of edge-shared $[UO_2F_5]$ pentagonal bipyramids. The one-dimensional phase, $(C_4N_2H_{12})_2U_2F_{12} \cdot H_2O$ (UFO-9), is built up from chains of uranium(IV), coordinated by eight fluorine atoms, whereas the two-dimensional compound, $(C_4N_2H_{12})_2(U_2O_4F_5)_4 \cdot 11H_2O$ (UFO-10), contains layers of fluorine bridged uranium(VI) pentagonal bipyramids. The framework material, $(C_4N_2H_{12})U_2O_4F_6$ (MUF-1), is built up from edge-shared $[UO_2F_5]$ dimers that are corner linked, forming three intersecting one-dimensional channels. MUF-1 also represents the first open-framework actinide material. In addition, the structural topologies of both UFO-10 and MUF-1 are completely unprecedented with respect to uranium materials.

Introduction

Hydrothermal reactions of inorganic reagents (oxides, sulfides, or halides) in the presence of aqueous acids and amines, under low temperature (T < 300 °C) and pressure (P < 100 atm) conditions, have proven very useful for the synthesis of new materials.[1−8] The careful control of the reaction conditions, in concert with the amine, has enabled researchers to synthesize a vast range of layered and microporous materials in which the cationic organic species is occluded within the anionic inorganic framework. The role of the organic molecule may be thought of as simply charge balancing or structure directing, i.e., "templating",[1,2,5] but the precise nature of these processes is not well understood.[6,9] Nonetheless, by varying the organic template, a diverse range of anionic framework topologies have been synthesized and structurally characterized. Continued interest in the synthesis of these organic−inorganic hybrid materials is driven by academic interests as well as potential industrial applications, such as heterogeneous catalysis,[8] molecular sieving, and ion-exchange.[4] Whereas the majority of new materials contain silicon, aluminum, and phosphorus,[6,10,11] researchers have successfully incorporated a variety of main group and transition metals into layered and three-dimensional frameworks.[12−17] We have been interested in extending this chemistry to the actinides, specifically uranium, attributable to

†Current address: Department of Chemistry, University of Houston, 4800 Calhoun Blvd., Houston, TX 77204.

(1) Breck, D. W. *Zeolite Molecule Sieves: Structure, Chemistry and Use*; Wiley and Sons: London, 1974.
(2) Barrer, R. M. *Hydrothermal Chemistry of Zeolites*; Academic Press: London, 1982.
(3) Lok, B. M.; Cannon, T. R.; Messina, C. A. *Zeolites* **1983**, *3*, 282−291.
(4) Clearfield, A. *Chem. Rev.* **1988**, *88*, 125−148.
(5) Szostak, R. *Molecular Sieves: Principles of Synthesis and Identification*; Reinhold: New York, 1989.
(6) Davis, M. E.; Lobo, R. F. *Chem. Mater.* **1992**, *4*, 756−768.
(7) Gies, H.; Marler, B. *Zeolites* **1992**, *12*, 42−49.
(8) Venuto, P. B. *Microporous Mater.* **1994**, *2*, 297−411.
(9) Francis, R. J.; O'Hare, D. *J. Chem. Soc., Dalton Trans.* **1998**, 3133−3148.
(10) Wilson, S. T.; Lok, B. M.; Messina, C. A.; Cannon, T. R.; Flanigen, E. M. *ACS Symp. Ser.* **1983**, *218*, 79.
(11) Flanigen, E. M.; Patton, R. L.; Wilson, S. T. *Stud. Surf. Sci. Catal.* **1988**, *37*, 13−27.
(12) Gier, T. E.; Stucky, G. D. *Nature* **1991**, *349*, 508−510.
(13) Ferey, G. *J. Fluorine Chem.* **1995**, *72*, 187−193.
(14) Chippindale, A. M.; Brech, S. J.; Cowley, A. R.; Simpson, W. M. *Chem. Mater.* **1996**, *8*, 2259−2264.
(15) Haushalter, R. C.; Mundi, L. A. *Chem. Mater.* **1992**, *4*, 31−48.
(16) Annen, M. J.; Davis, M. E.; Higgins, J. B.; Schlenker, J. L. *J. Chem. Soc., Chem. Commun.* **1991**, 1175−1176.
(17) Feng, P. Y.; Bu, X. H.; Stucky, G. D. *Nature* **1997**, *388*, 735.

10.1021/ja992145f CCC: $18.00
Published on Web 10/30/1999

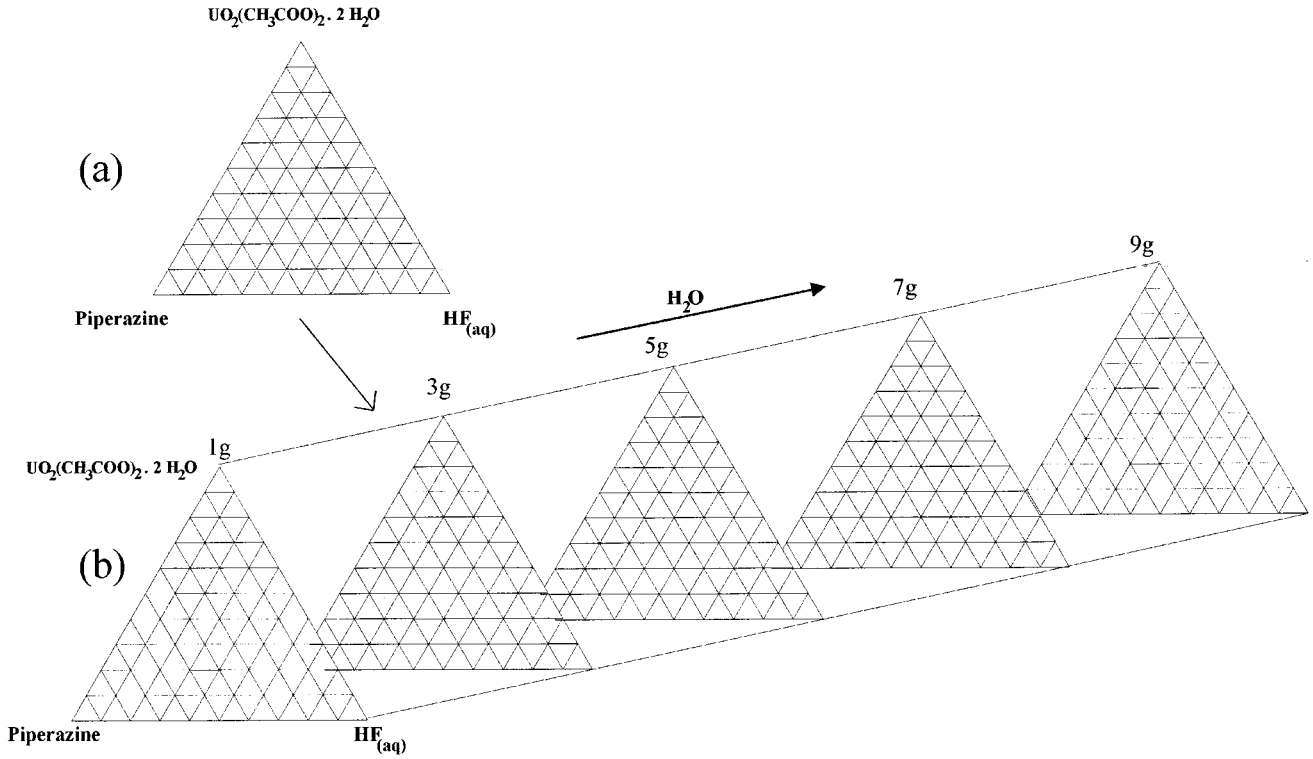

Figure 1. (a) Composition space of the $UO_2(CH_3COO)_2 \cdot 2H_2O/HF_{(aq)}$/piperazine system. (b) Composition prism, constructed from five composition spaces. Each space comprised reactions with a different amount of "excess" H_2O.

its proven catalytic properties,[18] and have recently published the syntheses and structures of a variety of porous U^{IV} and U^{VI} materials.[19−21]

For almost all of the many applications envisioned, phase purity is an essential prerequisite, and a degree of control over the framework architecture would be very desirable. Our approach has been to identify key reaction variables and systematically explore their influence experimentally, to determine stability regions where particular compounds can be synthesized in phase-pure form. One manner in which these stability regions may be determined is through the use of composition space diagrams (see Figure 1a),[22−24] which are graphically similar to ternary phase diagrams. We have extended this concept to include the quantity of solvent, in our case H_2O, as a fourth variable and in doing so have altered the two-dimensional composition space to a three-dimensional compositional prism,[20] where the prism axis is the amount of H_2O added to each reaction (see Figure 1b).

We have used the composition space and prism approach with the $UO_2(CH_3COO)_2 \cdot 2H_2O/HF_{(aq)}$/piperazine system and have succeeded in determining stability regions wherein new uranium materials, $(C_4N_2H_{12})UO_2F_4 \cdot 3H_2O$ (UFO-8a and -8b), $(C_4N_2H_{12})_2U_2F_{12} \cdot H_2O$ (UFO-9), $(C_4N_2H_{12})_2(U_2O_4F_5)_4 \cdot 11H_2O$ (UFO-10), and $(C_4N_2H_{12})U_2O_4F_6$ (MUF-1), are synthesized in phase-pure form.[25] These materials span the range of dimensionalities from molecular, zero-dimensional (0-D; UFO-8a and -8b) through framework, three-dimensional (3-D; MUF-1). The stability regions observed for each phase are discussed and rationalized through the composition space and prism diagrams.

Experimental Section

Caution: Although all uranium materials used in these experiments were depleted, care and good laboratory practice should always be used when handling any uranium-containing material!

Reagents. The chemicals in this work were used as obtained without further purification. Piperazine (95%) was from Aldrich, and the $HF_{(aq)}$ (40% solution) was from Fissions. The uranium reagent, $UO_2(CH_3COO)_2 \cdot 2H_2O$, was synthesized as previously reported.[21]

Syntheses. $(C_4N_2H_{12})UO_2F_4 \cdot 3H_2O$ **(UFO-8a)**: 0.406 g (1.0×10^{-3} mol) of $UO_2(CH_3COO)_2 \cdot 2H_2O$, 0.258 g ($3.0 \times 10^{-3}$ mol) of piperazine, 0.43 g (2.1×10^{-2} mol) of $HF_{(aq)}$, and 1 g of H_2O. Elemental analysis. Calcd: C, 10.42; H, 3.28; N, 6.07; F, 16.48. Exptl: C, 9.84; H, 3.72; N, 5.74; F, 16.28.

$(C_4N_2H_{12})UO_2F_4 \cdot 3H_2O$ **(UFO-8b)**: 0.406 g (1.0×10^{-3} mol) of $UO_2(CH_3COO)_2 \cdot 2H_2O$, 0.474 g ($5.5 \times 10^{-3}$ mol) of piperazine, 0.98 g (4.9×10^{-2} mol) of $HF_{(aq)}$, and 1 g of H_2O. Elemental analysis. Calcd: C, 10.42; H, 3.28; N, 6.07. Exptl: C, 9.96; H, 3.57; N, 5.67.

$(C_4N_2H_{12})_2U_2F_{12} \cdot H_2O$ **(UFO-9)**: 0.406 g (1.0×10^{-3} mol) of $UO_2(CH_3COO)_2 \cdot 2H_2O$, 0.689 g ($8.0 \times 10^{-3}$ mol) of piperazine, 0.80 g (4.0×10^{-2} mol) of $HF_{(aq)}$, and 1 g of H_2O. Elemental analysis. Calcd: C, 10.94; H, 3.21; N, 6.38. Exptl: C, 10.52; H, 3.31; N, 6.02.

$(C_4N_2H_{12})_2(U_2O_4F_5)_4 \cdot 11H_2O$ **(UFO-10)**: 0.406 g (1.0×10^{-3} mol) of $UO_2(CH_3COO)_2 \cdot 2H_2O$, 0.120 g ($1.4 \times 10^{-3}$ mol) of piperazine, 0.12 g (6.0×10^{-3} mol) of $HF_{(aq)}$, and 1 g of H_2O. Elemental analysis. Calcd: C, 3.30; H, 1.59; N, 1.92; F, 13.04. Exptl: C, 3.31; H, 1.86; N, 1.87; F, 12.90.

$(C_4N_2H_{12})U_2O_4F_6$ **(MUF-1)**: 0.406 g (1.0×10^{-3} mol) of $UO_2(CH_3COO)_2 \cdot 2H_2O$, 0.861 g ($1.0 \times 10^{-2}$ mol) of piperazine, 1.15 g ($5.7 \times$

(18) Hutchings, G. J.; Heneghan, C. S.; Hudson, I. D.; Taylor, S. H. *Nature* **1996**, *384*, 341−343.

(19) Francis, R. J.; Halasyamani, P. S.; O'Hare, D. *Angew. Chem., Int. Ed.* **1998**, *37*, 2214−2217. Francis, R. J.; Halasyamani, P. S.; O'Hare, D. *Chem. Mater.* **1998**, *10*, 3131−3139.

(20) Francis, R. J.; Halasyamani, P. S.; Bee, J. S.; O'Hare, D. *J. Am. Chem. Soc.* **1999**, *121*, 1609−1610.

(21) Halasyamani, P. S.; Francis, R. J.; Walker, S. M.; O'Hare, D. *Inorg. Chem.* **1999**, *38*, 271−279.

(22) Halasyamani, P. S.; Willis, M. J.; Lundquist, P. M.; Stern, C. L.; Wong, G. K.; Poeppelmeier, K. R. *Inorg. Chem.* **1996**, *35*, 1367−1371.

(23) Harrison, W. T. A.; Dussack, L. L.; Jacobson, A. J. *J. Solid State Chem.* **1996**, *125*, 234−239.

(24) Norquist, A. J.; Heier, K. R.; Stern, C. L.; Poeppelmeier, K. R. *Inorg. Chem.* **1998**, *37*, 6495−6501.

(25) A few comments are necessary regarding the nomenclature used. The molecular, one- and two-dimensional materials are termed UFO-# (Uranium Fluoride from Oxford), whereas the framework,three-dimensional phase is called MUF-# (Microporous Uranium Fluoride).

Table 1. Selected Crystallographic Data for UFO-8a, UFO-8b, UFO-9, UFO-10, and MUF-1

formula	$C_4H_{18}N_2O_5F_4U$ (UFO-8a)	$C_4H_{18}N_2O_5F_4U$ (UFO-8b)	$C_8H_{26}N_4O_1F_{12}U_2$ (UFO-9)	$C_8H_{46}N_4O_{27}F_{20}U_8$ (UFO-10)	$C_4H_{12}N_2O_4F_6U_2$ (MUF-1)
fw	488.23	488.23	898.35	2914.69	742.20
crystal color	yellow	yellow	green	yellow	yellow
crystal size (mm)	0.15 × 0.15 × 0.18	0.12 × 0.12 × 0.18	0.03 × 0.03 × 0.54	0.005 × 0.007 × 0.02	0.12 × 0.12 × 0.15
temperature (K)	150.0	200.0	150.0	150.0	150.0
crystal system	monoclinic	triclinic	monoclinic	monoclinic	monoclinic
space group	$P2_1/n$ (No. 14)	$P\bar{1}$ (No. 2)	$C2/m$ (No. 12)	$P2_1/n$ (No. 14)	$C2/c$ (No. 15)
a (Å)	8.503(1)	11.983(1)	13.017(1)	17.309(5)	9.108(1)
b (Å)	9.847(1)	8.751(1)	12.379(1)	12.092(5)	10.059(1)
c (Å)	15.009(1)	6.412(1)	6.651(1)	24.399(7)	13.633(1)
α (deg)	90	91.530(4)	90	90	90
β (deg)	100.17(3)	112.143(4)	107.68(1)	90.47(2)	97.023(1)
γ (deg)	90	98.444(3)	90	90	90
V (Å^3), Z	1236.94(3), 4	613.60(3), 2	1021.10(3), 2	5106(3), 4	1239.6(2), 4
μ (cm^{-1}), Mo Kα	131.81	132.8	159.51	96.28	261.79
ρ_{calc} (g/cm^3)	2.622	2.643	2.922	3.792	3.977
$R(F)^a$	0.036	0.047	0.029	0.084	0.041
$R_w(F^2)^b$	0.085	0.117	0.079	0.161	0.105

[a] $R = \sum||F_o| - |F_c||/\sum|F_o|$. [b] $R_w = [\sum w(|F_o^2| - |F_c^2|)^2/\sum w(F_o^2)^2]^{1/2}$.

10^{-2} mol) of $HF_{(aq)}$, and 1 g of H_2O. Elemental analysis. Calcd: C, 6.47; H, 1.63; N, 3.77; F, 16.48. Exptl: C, 6.54; H, 1.79; N, 3.77; F, 16.08.

The reagent amounts listed above were placed in separate 23-mL Teflon-lined autoclaves that were closed, heated at 180 °C for 24 h, and cooled slowly at 6 °C h^{-1} to room temperature. For UFO-8a, -8b, -10, and MUF-1 yellow crystals were recovered, whereas for UFO-9 green needles were synthesized. The five materials, UFO-8a, -8b, -9, -10, and MUF-1, were synthesized in 84%, 91%, 79%, 64%, and 75% yields, respectively, based on uranium. Powder X-ray diffraction patterns on the synthesized phases are in excellent agreement with the generated pattern from the single-crystal data (see Supporting Information).

X-ray Crystallographic Studies. Crystallographic data for all the materials except UFO-10 were acquired on an Enraf-Nonius DIP 2000 image-plate diffractometer using graphite-monochromated Mo Kα (λ = 0.710 73 Å) radiation with a step of 2°/frame, θ_{max} = 26°. The crystals were mounted on a glass fiber under paratone oil and cooled on the diffractometer. Each frame was collected, indexed, and processed using DENZO,[26] and the files were scaled together using SCALEPACK.[26] For UFO-10, single-crystal data were acquired at station 9.8 of the CLRC Daresbury Laboratory on a Bruker AXS SMART CCD area-detector diffractometer.[27,28] Reflection intensities were integrated by standard procedures, allowing for the plane-polarized nature of the primary synchrotron beam, and corrections were applied semiempirically for absorption and incident beam decay.[29,30] For all of the structures, the heavy atoms' positions were determined using SIR92,[31] and other non-hydrogen atoms were refined using SHELXL-93.[32] All non-hydrogen atoms found by Fourier difference maps were refined with anisotropic thermal parameters, except for $(C_4N_2H_{12})U_2O_4F_6$ (MUF-1), where the piperazinium cation was refined isotropically, using full-matrix least-squares procedures on F_o^2 with $I > 2\sigma(I)$. Hydrogen atoms were fixed in geometrically idealized positions and allowed to ride on their attached carbon or nitrogen atom with isotropic thermal parameters according to the atom to which they were connected (these were not refined). The assignment of the nitrogen atoms on the piperazine ring was inferred from hydrogen-bonding interactions with either the fluoride or oxygen atoms. An empirical data correction using XABS2[33] was applied before merging symmetry equivalent reflections. All calculations were performed using the WinGX-98[34] crystallographic software package. Selected crystallographic data for each compound are given in Table 1. Fractional atomic coordinates, thermal parameters, and a list of pertinent bond lengths are given in the Supporting Information.

Ion-Exchange Experiments. Ion-exchange reactions were attempted by stirring ca. 100 mg of either UFO-8a, -8b, -9, -10, or MUF-1 in 10 mL of 2 M aqueous solution of the following metal salts: $NaNO_3$, KNO_3, RbF, CsCl, $Mg(NO_3)\cdot 6H_2O$, $Ca(NO_3)_2\cdot 4H_2O$, $SrCl_2$, or $BaCl_2$. The reactions were performed at room temperature over a period of 24 h.

Infrared and Raman Spectroscopy. FTIR spectra were collected on a Perkin-Elmer FT 1710 spectrometer using Nujol mulls of samples pressed between KBr plates. Raman spectra were collected using a Dilor Labram laser spectrometer on crystals mounted on microscope slides.

Thermogravimetric Analysis. TGA measurements were performed on a Rheometric Scientific STA 1500H thermal analyzer. The samples were contained within platinum crucibles and heated at a rate of 5 °C min^{-1} from room temperature to 500 °C in static air.

Results and Discussion

Structural Diversity. One of the most impressive results of hydrothermal chemistry is the synthesis of materials with an astonishingly diverse range of structural characteristics. However, despite this diversity, there is often a lack of understanding of the relationships between the reaction conditions employed and the product obtained. For zeolites, microporous aluminosilicates, it has been demonstrated that increasing the synthesis temperature produces materials with lower intercrystalline void space. With microporous metal phosphates, a number of variables have been identified, such as pH, temperature, and pressure, all of which have been shown to influence the product. In both zeolites and metal phosphates, one factor that unquestionably affects the product is the organic template employed, usually an amine. It has been demonstrated that a small change in the amine's structure can result in the syntheses of strikingly

(26) Otwinowski, Z. In *Data Collection and Processing, Proceedings of the CCP4 study weekend*; Otwinowski, Z., Ed.; Daresbury Laboratory: Warrington, UK, 1993.

(27) Cernik, R. J.; Clegg, W.; Catlow, C. R. A.; Bushnell-Wye, G.; Flaherty, J. V.; Greaves, G. N.; Hamichi, M.; Borrows, I. D.; Taylor, D. J.; Teat, S. J. *J. Synchrotron Radiat.* **1997**, *4*, 279−286.

(28) Clegg, W.; Elsegood, M. J. R.; Teat, S. J.; Redshaw, C.; Gibson, V. C. *J. Chem. Soc., Dalton Trans.* **1998**, 3037−3039.

(29) *SMART (control) and SAINT (integration) software*, 4th ed.; Bruker AXS Inc.: Madison, WI, 1994.

(30) Sheldrick, G. M. In *SADABS*; Sheldrick, G. M., Ed.; University of Göttingen: Göttingen, Germany, 1997.

(31) Altomare, A.; Cascarano, G.; Giacovazzo, C.; Guagliardi, A. *J. Appl. Crystallogr.* **1994**, *27*, 343−350.

(32) Sheldrick, G. M. In *SHELXL-93−A program for crystal structure refinement*; Sheldrick, G. M., Ed.; University of Göttingen: Göttingen, Germany, 1993.

(33) Parkin, S.; Moezzi, B.; Hope, H. *J. Appl. Crystallogr.* **1995**, *28*, 53−56.

(34) Farrugia, L. J. In *WinGX−An integrated system of publically available windows programs for the solution, refinement, and analysis of single-crystal X-ray diffraction data*; Farrugia, L. J., Ed.; University of Glasgow: Glasgow, UK, 1998.

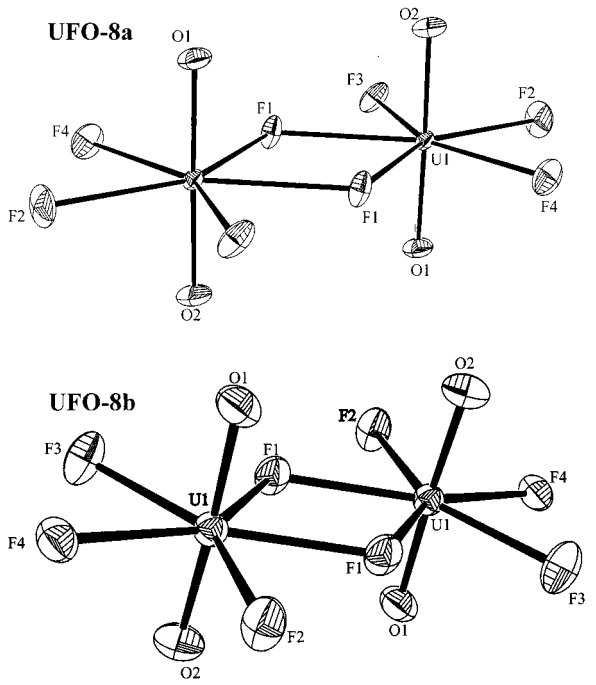

Figure 2. ORTEP (50% probability ellipsoids) of the dimer in $(C_4N_2H_{12})UO_2F_4{\cdot}3H_2O$ (UFO-8a and -8b), $[U_2O_4F_8]^{4-}$.

different materials. This is the situation for the gallium phosphate oxyfluoride[13] and reduced molybdenum phosphate families[15] of organically templated microporous materials. In the former system, a variety of three-dimensional microporous phases have been synthesized by using different amine templates, whereas in the molybdenum phosphate family, the products included molecular, one-, two-, and three-dimensional compounds, again by using different templates. We recently demonstrated that molecular, one-, or two-dimensional phases could be synthesized, in phase-pure form, using 2-methylpiperazine as the template and UO_2 and $HF_{(aq)}$ as reagents.[20] In the $UO_2/HF_{(aq)}$/2-methylpiperazine system, we observed a direct relationship between the acidity of the reaction and the dimensionality of the product phase. Described below are another series of materials, all synthesized using $UO_2(CH_3COO)_2{\cdot}2H_2O$, $HF_{(aq)}$, and piperazine, whose dimensionalities span the entire range from molecular, 0-D to framework, 3-D.

Zero-Dimensional Phase. Two polymorphic molecular phases, $(C_4N_2H_{12})UO_2F_4{\cdot}3H_2O$ (UFO-8a and -8b), are observed in the $UO_2(CH_3COO)_2{\cdot}2H_2O/HF_{(aq)}$/piperazine system. The hydrothermal reaction that produces UFO-8a initially generates a clear yellow-green solution (pH 4.0). Upon the solution standing for several hours, yellow prismatic crystals are observed. However, UFO-8b is synthesized as greenish-yellow rodlike crystals immediately following the hydrothermal reaction together with a mother liquor of pH 2.5. Both polymorphs of UFO-8 are molecular phases consisting of UO_2F_5 pentagonal bipyramids that share an edge to form $[U_2O_4F_8]^{4-}$ dimers (see Figure 2). Within each dimer, the U^{VI} is bonded axially to two oxygens and equatorially to five fluorines, of which two bridge and three remain singly bonded. Thus, in connectivity terms, each uranium can be considered an $[UO_{2/1}F_{2/2}F_{3/1}]^{2-}$ anion. Common to all U^{VI} oxo complexes, a nearly linear uranyl unit, O═U═O = 178.8(2)° and 177.3(3)° for UFO-8a and -8b, respectively, is observed with U═O bond distances ranging from 1.779(5) to 1.804(8) Å. The bridging and terminal U−F distances range from 2.244(6) to 2.368(4) Å. Stability is imparted to the structure through a host of hydrogen-bonding interactions, not only between the protonated piperazine cation and the $[U_2O_4F_8]^{4-}$ dimer but also between the template and the occluded H_2O molecules. The main structural difference between UFO-8a and -8b is observed through their hydrogen-bonding networks. In UFO-8a, the hydrogen-bonding interactions serve to link the dimers along the [0 1 0], [0 0 1], [0 1 1], and [0 1 −1] directions, whereas in UFO-8b, the hydrogen-bonding interactions are observed along [1 0 0], [0 1 0], [1 1 0], and [−1 1 0] (see Figure 3). Although UFO-8a and -8b are new materials, the $[U_2O_4F_8]^{4-}$ dimer has been observed previously in both $Rb_2UO_2F_4{\cdot}H_2O$[35] and $Cs_2UO_2F_4{\cdot}H_2O$.[36] The bond distances and angles observed in UFO-8a and -8b are in excellent agreement with the aforementioned compounds. Bond valence[37] calculations on the U^{VI} cations in UFO-8a and -8b, using parameters calculated by Burns et al.,[38] resulted in values of 5.40 and 5.63.

One-Dimensional Phase. Unlike the other compounds in this report, $(C_4N_2H_{12})_2U_2F_{12}{\cdot}H_2O$ (UFO-9) is a U^{IV} material. UFO-9 has a one-dimensional structure with uranium fluoride chains built up from edge-sharing polyhedra. The uranium fluoride chains run along the [0 0 1] direction and are separated by piperazinium cations and occluded water molecules. Strong ionic and hydrogen bonds between the uranium fluoride chains and the piperazinium cations impart stability to the structure. Within the chains, each uranium cation is coordinated to eight fluorine atoms in distorted trigonal prismatic arrangement. Each uranium fluoride trigonal prism shares two edges with adjacent polyhedra to form the chains. Thus, each U^{IV} trigonal prism contains four terminal and four bridging fluorine atoms and can be described in connectivity terms as a $[UF_{4/2}F_{4/1}]^{2-}$ anion. The terminal and bridging U−F bond distances range from 2.163(5) to 2.270(7) and from 2.295(5) to 2.455(6) Å respectively, with an intrachain U−U distance of 4.052(1) Å. Similar to UFO-8a and -8b, a number of N−H···F hydrogen-bonding interactions between the uranium fluoride chains and the protonated piperazine molecules are observed. These interactions form a diamond-shaped network, with a ca. 7 Å × 8 Å cavity (see Figure 4), that is occupied by the occluded H_2O molecules. We have shown through thermogravimetric and powder XRD experiments that, upon dehydration, UFO-9 retains crystallinity. Additionally, rehydration and conversion back to UFO-9 occur at room temperature over several hours. Bond valence[37,38] calculations on the U^{IV} cation in UFO-9 resulted in a value of 4.13.

Two-Dimensional Phase. The layered phase, $(C_4N_2H_{12})_2(U_2O_4F_5)_4{\cdot}11H_2O$ (UFO-10), exhibits an unprecedented topology with respect to uranium materials. This two-dimensional compound consists of anionic sheets of linked UO_2F_5 pentagonal bipyramids, with each U^{VI} coordinated to two oxygens and five fluorines. As with UFO-8a, -8b and other U^{VI}−oxo complexes, a nearly linear uranyl unit is observed with O═U═O angles ranging from 177.6(5) to 179.5(5)° and U═O distances ranging from 1.711(10) to 1.828(10) Å. The U−F distances range from 2.266(8) to 2.352(8) Å. Each U^{VI} pentagonal bipyramid is corner linked through all five fluorines to form the anionic layer, with intra- and interlayer U−U distances ranging from 4.351(7) to 4.553(7) and 8.385(8) Å, respectively. In connectivity terms, each U^{VI} can be described as an $[UO_{2/1}F_{5/2}]^{0.5-}$ anion. Polyhedral and ball-and-stick representations of UFO-10 perpendicular to the layer are given in Figure 5. As can be seen in Figure 5, every UO_2F_5 pentagonal bipyramid is corner linked to five

(35) Brusset, H.; Quo Dao, N.; Rubinstein-Auban, A. *Acta Crystallogr. B* **1972**, *28*, 2617−2619.
(36) Quy Dao, N. *Acta Crystallogr. B* **1972**, *28*, 2011−2015.
(37) Brown, I. D.; Altermatt, D. *Acta Crystallogr.* **1985**, *B41*, 244.
(38) Burns, P. C.; Ewing, R. C.; Hawthorne, F. C. *Can. Miner.* **1997**, *35*, 1551−1570.

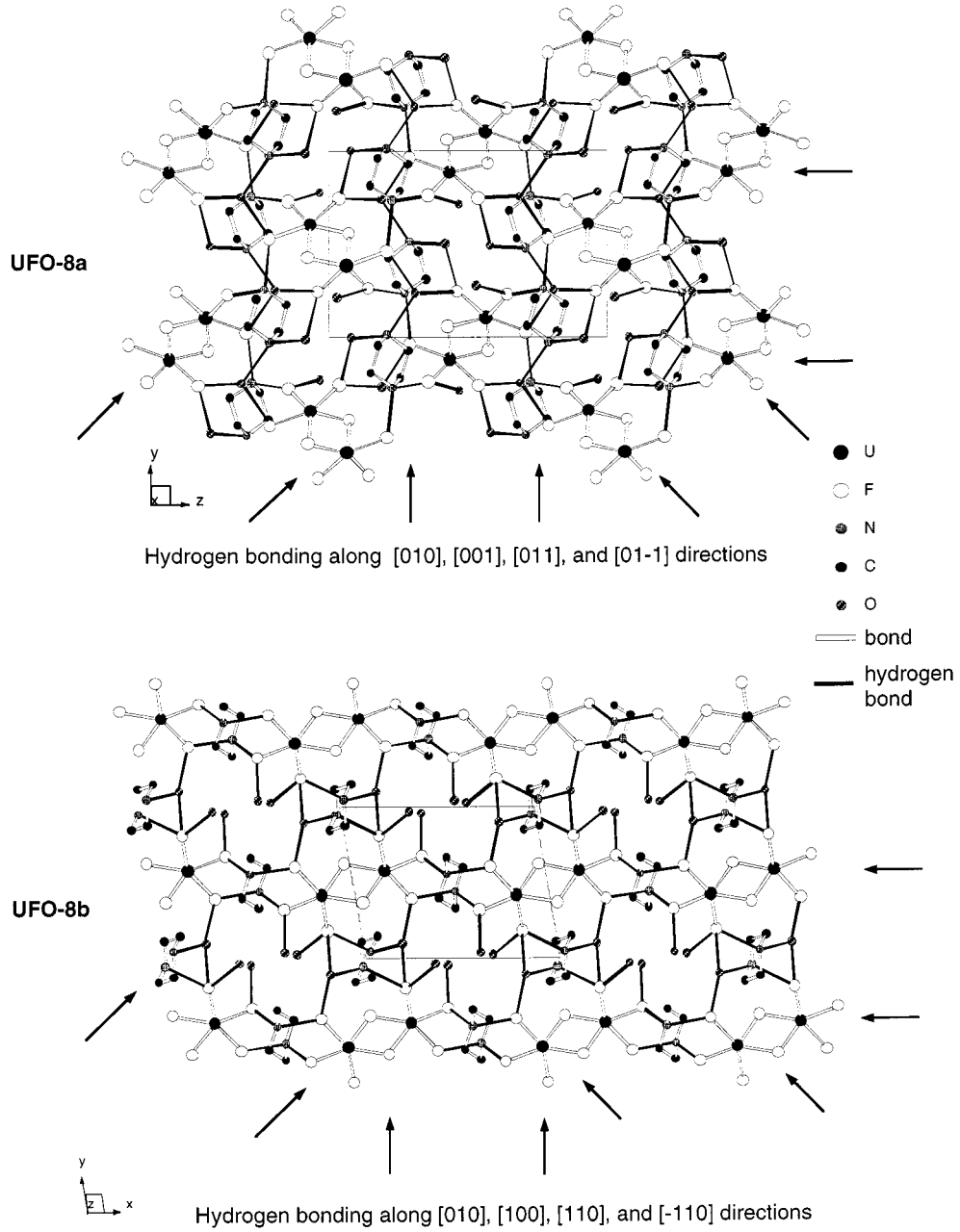

Figure 3. Ball-and-stick representation of hydrogen-bonding interactions in UFO-8a (top) and -8b (bottom). Hydrogen-bonding chains are observed along the [0 1 0], [0 0 1], [0 1 1], and [0 1 −1] directions in UFO-8a, whereas in UFO-8b the chains occur along the [0 1 0], [1 0 0], [1 1 0], and [−1 1 0] directions (uranyl oxygens removed for clarity).

identical pentagonal bipyramids. The uranium fluoride layers are separated by the piperazinium cation and the occluded water molecules (see Figure 6). The layer itself is not flat but is slightly puckered. Interestingly, and unlike UFO-8a, -8b, and -9, hydrogen-bonding interactions are not observed between the piperazinium cation and the layer but rather only between the template and the occluded water molecules. Bond valence[37,38] calculations on the U^{VI} cations in UFO-10 resulted in values ranging from 5.15 to 5.53.

Three-Dimensional Phase. Probably the most interesting material in this report is $(C_4N_2H_{12})U_2O_4F_6$ (MUF-1).[39] MUF-1 represents the first example of an open-framework material containing an actinide. MUF-1 is a three-dimensional material consisting of corner- and edge-shared uranium pentagonal bipyramids. Each U^{VI} is axially bonded to two oxygens, forming a uranyl unit (U═O = 1.773(4) and 1.779(4) Å) with a O═U═O bond angle of 178.37(2)°. Equatorially, each U^{VI} is bonded to five fluorines, four of which bridge to an adjacent uranium, with U−F bonds ranging from 2.274(1) to 2.353(4) Å, whereas the fifth fluorine is singly bonded (U−F = 2.196(8) Å). Thus, in connectivity terms, each uranium pentagonal bipyramid can be described as a $[UO_{2/1}F_{4/2}F_{1/1}]^-$ anion, with charge balance maintained by a piperazinium cation.

This framework structure can be best described as comprising edge-shared UO_2F_5 pentagonal bipyramid dimers that are corner linked to form the three-dimensional network. This network contains three intersecting one-dimensional channels consisting of 10-, 8-, and 6-membered rings (10-MRs, 8-MRs, and 6-MRs) of pentagonal bipyramids. Each side of the ring is defined by a line drawn between two adjacent uranium atoms, i.e., edge- or corner-linked polyhedra. The edges of the 10-MR channel are built up from six corner-linked dimers (see Figure 7). The 10-

(39) Halasyamani, P. S.; Walker, S. M.; O'Hare, D. *J. Am. Chem. Soc* **1999**, *121*, 7415−7416.

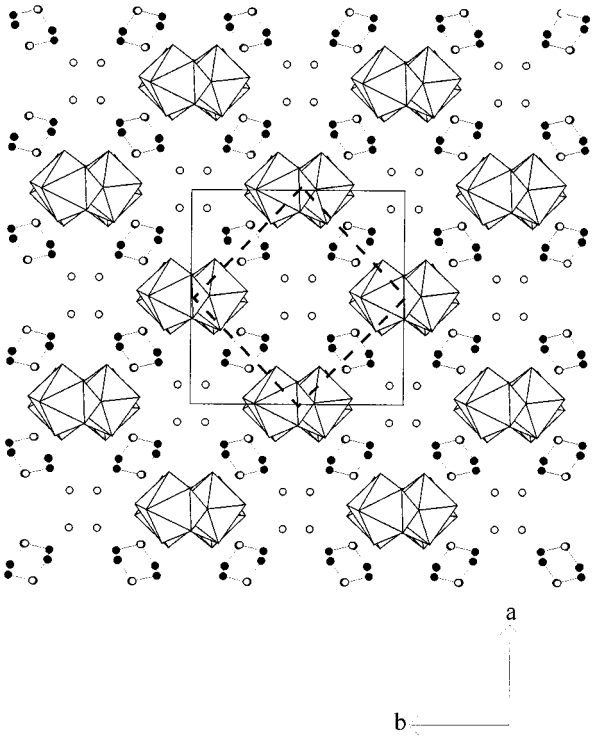

Figure 4. Polyhedral representation of $(C_4N_2H_{12})_2U_2F_{12}\cdot H_2O$ (UFO-9) viewed down the [0 0 1] direction. The dashed line represents the diamond-shaped network formed by the chains.

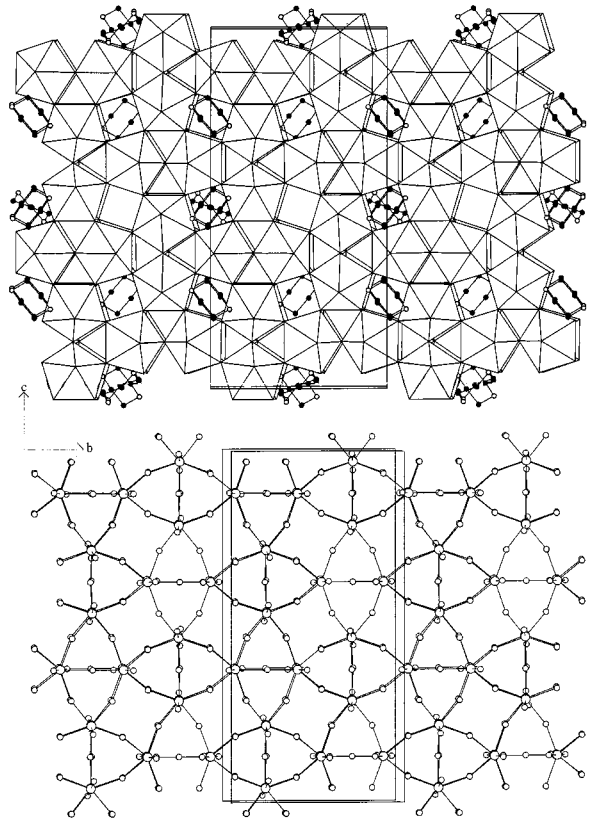

Figure 5. Polyhedral (top) and ball-and-stick (bottom) representations of $(C_4N_2H_{12})_2(U_2O_4F_5)_4\cdot 11H_2O$ (UFO-10) viewed perpendicular to the layer, along the [1 0 0] direction. Note the triangular and square "holes" formed by the $[UO_{2/1}F_{5/2}]^{0.5-}$ topology.

MR channel is elliptical in nature with a pore size of 5.5 Å × 12.2 Å, as defined by the shortest oxygen−oxygen (or fluorine−fluorine) contact, using atomic radii from Shannon.[40] Perpendicular to and intersecting the 10-MR channel are the 8-MR pores, which run in the [0 0 1] direction (see Figure 8). The edges of this channel contain four corner-linked UO_2F_5 dimers. Although the channel may seem rather spherical, the pore size is 2.6 Å × 5.5 Å, owing to the two uranyl bonds that point into the channel. The third one-dimensional channel is a 6-MR pore, whose edges are built up from six edge-shared UO_2F_5 dimers (see Figure 9). The pore, which runs down the [0 1 0] direction, is perpendicular to the 8-MR channel but intersects the 10-MR channel at a 45° angle. The 6-MR channel has a pore size of 2.7 Å × 4.1 Å. The piperazinium cations are observed only in

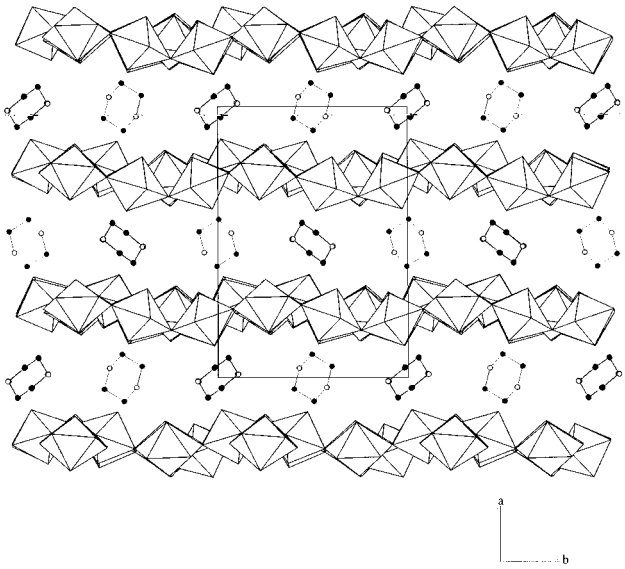

Figure 6. Polyhedral representation of $(C_4N_2H_{12})_2(U_2O_4F_5)_4\cdot 11H_2O$ (UFO-10) parallel to the layers, along the [0 0 1] direction (occluded water molecules removed for clarity).

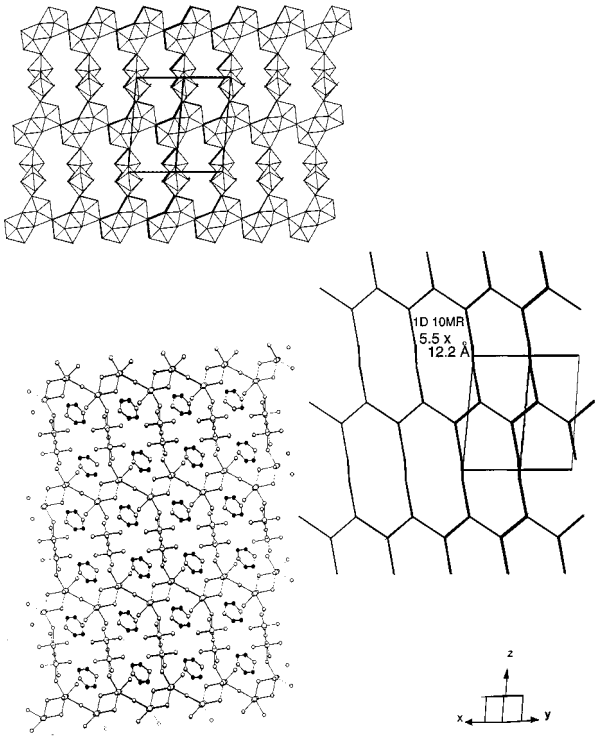

Figure 7. Polyhedral, wire, and ball-and-stick representation of the 10-membered ring in $(C_4N_2H_{12})U_2O_4F_6$ (MUF-1). In the wire diagram, each side of the channel is a U−U nearest-neighbor contact.

(40) Shannon, R. D. *Acta Crystallogr.* **1976**, *A32*, 751−760.

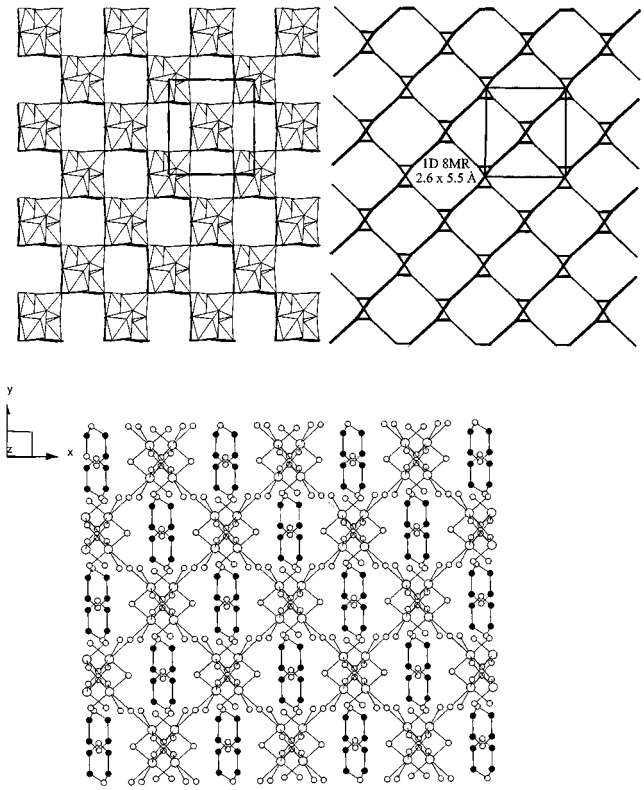

Figure 8. Polyhedral, wire, and ball-and-stick representation of the 8-membered ring in $(C_4N_2H_{12})U_2O_4F_6$ (MUF-1). In the wire diagram, each side of the channel is a U−U nearest-neighbor contact.

the 10-MR and 8-MR channels, with N−H···F hydrogen bonding observed with terminal and bridging fluorine atoms. Bond valence[37,38] calculations on the U^{VI} cation in MUF-1 resulted in a value of 5.45. Thermogravimetric experiments revealed that MUF-1 is stable only up to 350 °C, at which point the template is removed and the framework decomposes to U_3O_8.

Composition Spaces and Prism. The composition spaces and prism for $UO_2(CH_3COO)_2 \cdot 2H_2O/HF_{(aq)}$/piperazine will be discussed shortly, but before we delve into the details of the system, a few comments are necessary. Although the composition space is graphically similar to a ternary phase diagram, it cannot be treated as such since amorphous products as well as the solution phase are not accounted for. In addition, another equally important distinction must be drawn. In a composition space, if the molar ratio between reagents, excluding excess water, is held constant but the number of moles is increased (or decreased), the synthetic result will change. This is because a greater (or lesser) amount of reagents is being placed into a finite volume as well as a fixed amount of water, changing both the solubility of the reagents and the total pressure. The analogous situation does not occur in a ternary phase diagram, where an increase (or decrease) in the initial molar amounts will simply produce proportionately more (or less) of the product(s). However, even with the above caveat, the composition space and prism construction provide an easily understood manner in which to delineate stability regions of specific phases. To construct each composition space, 19 separate reactions were performed using 10^{-3} mol (0.406 g) of $UO_2(CH_3COO)_2 \cdot 2H_2O$ in each reaction and a constant amount of water. The composition prism is created by varying the amount of water in each reaction, such that the prism axis represents the excess water added (see Figure 1).

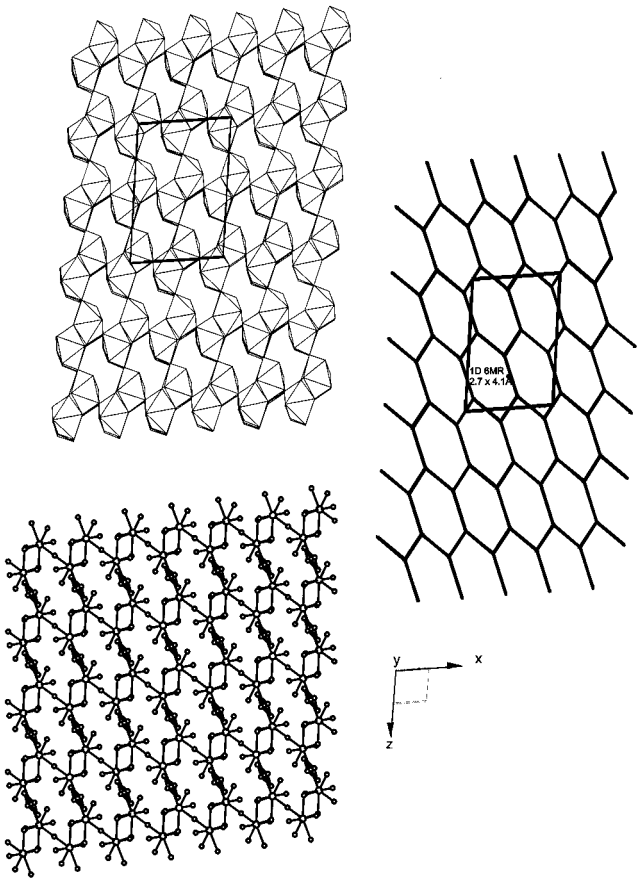

Figure 9. Polyhedral, wire, and ball-and-stick representation of the six-membered ring in $(C_4N_2H_{12})U_2O_4F_6$ (MUF-1). In the wire diagram, each side of the channel is a U−U nearest-neighbor contact.

As can be seen in Figure 10, the composition spaces and prism for the $UO_2(CH_3COO)_2 \cdot 2H_2O/HF_{(aq)}$/piperazine system are very complex. Pure phases are represented as "open" symbols, ○, +, △, ☆ or ×, whereas mixtures are given as "filled"' symbols, ●, †, ▲, ★, ■, or ⟩ (see the key at the bottom right of the figure). The predominant phase observed throughout the prism is the three-dimensional compound, $(C_4N_2H_{12})U_2O_4F_6$ (MUF-1). This material can be synthesized in phase-pure form, represented as ×, under similar molar reagent ratios, and in a wide range of H_2O concentrations. The molecular phases $(C_4N_2H_{12})UO_2F_4 \cdot 3H_2O$ (UFO-8a and -8b) are found either as pure phases (○ and +, respectively) or as mixtures with each other (†), MUF-1 (●), or UFO-9 (▲). In all instances, the molecular phases are found in the piperazine-rich end of the composition spaces. The stability regions for UFO-8a and -8b increase in size from the 1g composition space to the 5g composition space, and then decrease in the 7g and 9g spaces. The one-dimensional phase, $(C_4N_2H_{12})_2U_2F_{12} \cdot H_2O$ (UFO-9), is found as a pure phase only in the 1g composition space. Where the compound is observed as a mixture, the material is found with either UFO-8a (⟩), -8b (▲), or both (■). Similar to the stability region for UFO-9, the two-dimensional phase, $(C_4N_2H_{12})_2(U_2O_4F_5)_4 \cdot 11H_2O$ (UFO-10), is found only in the 1g and 3g composition spaces. However, unlike UFO-9, UFO-10 is synthesized in the uranium acetate-rich end of the spaces and is found as a pure phase (☆) or as a mixture with MUF-1 (★).

The stability regions determined for UFO-8a and -8b, -9, -10, and MUF-1 reveal a great deal regarding the chemistry of the system. The only composition space where all four compounds are observed, in phase-pure form, is the 1g space (see Figure 11). (As UFO-8a and 8b are polymorphs, they are counted

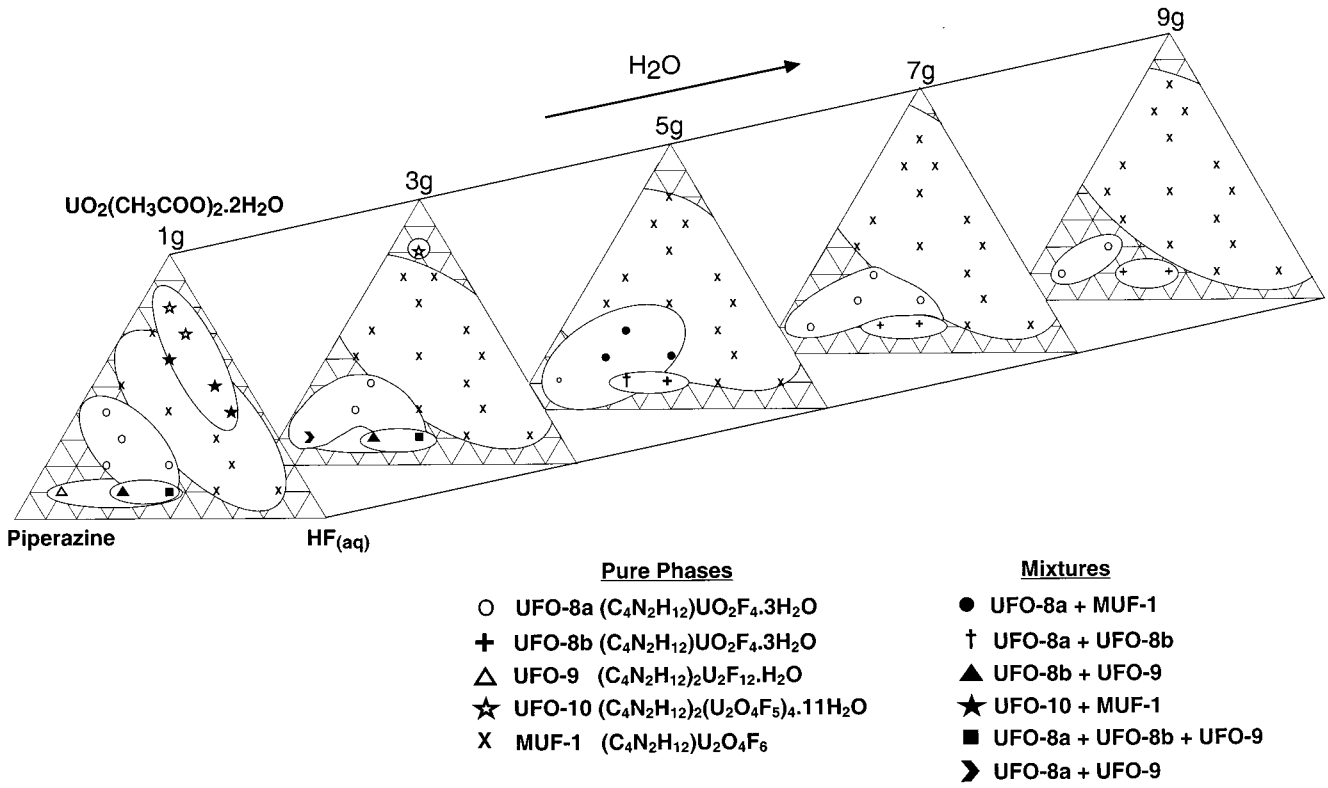

Figure 10. Composition prism for the $UO_2(CH_3COO)_2 \cdot 2H_2O/HF_{(aq)}$/piperazine system. Pure phase syntheses are denoted by open symbols, whereas mixtures are given by closed symbols. Note that the reduced phase, $(C_4N_2H_{12})_2U_2F_{12} \cdot H_2O$ (UFO-9), and the fully fluorine-bridged phase, $(C_4N_2H_{12})_2(U_2O_4F_5)_4 \cdot 11H_2O$ (UFO-10), are observed only in the 1g and 3g composition spaces.

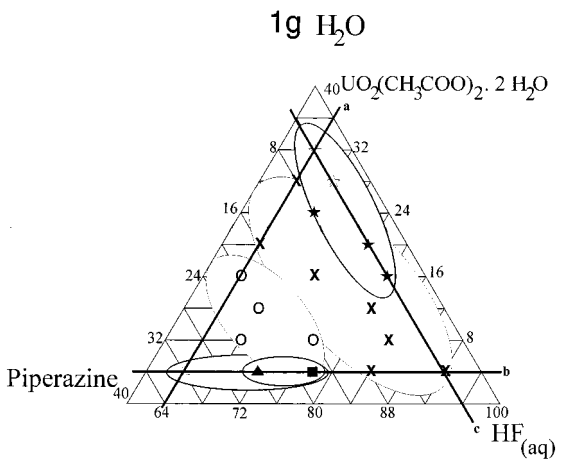

Figure 11. The 1g composition space for the $UO_2(CH_3COO)_2 \cdot 2H_2O/HF_{(aq)}$/piperazine system. The three lines added to the space, **a**, **b**, and **c**, represent synthesis under constant $HF_{(aq)}$, constant $UO_2(CH_3COO)_2 \cdot 2H_2O$, and constant piperazine, respectively.

together as one phase.) If we examine the piperazine−$UO_2(CH_3COO)_2 \cdot 2H_2O$ axis, the left edge of the triangle, an interesting observation may be made. Following this axis from the piperazine-rich corner toward the $UO_2(CH_3COO)_2 \cdot 2H_2O$-rich corner (the line marked as **a** in Figure 11) at a constant mole fraction of 0.64 $HF_{(aq)}$, we observe a change in phase from $(C_4N_2H_{12})_2U_2F_{12} \cdot H_2O$ (UFO-9) (△) → $(C_4N_2H_{12})UO_2F_4 \cdot 3H_2O$ (UFO-8a) (○) → $(C_4N_2H_{12})U_2O_4F_6$ (MUF-1) (×) → $(C_4N_2H_{12})_2(U_2O_4F_5)_4 \cdot 11H_2O$ (UFO-10) (☆) (see Figure 11). In the 1g space, the synthesis of UFO-9 is observed only in the piperazine-rich corner. UFO-9 is a templated U^{IV} fluoride, formed through the reduction of $UO_2(CH_3COO)_2 \cdot 2H_2O$. It is presumed that some of the piperazine is oxidized during the reaction. As the concentration of piperazine is decreased and $UO_2(CH_3COO)_2 \cdot 2H_2O$ is increased, UFO-8a, the molecular phase, is formed. Continuing toward the $UO_2(CH_3COO)_2 \cdot 2H_2O$-rich corner, the reaction product changes from MUF-1 to UFO-10. If we exclude the reduced phase, UFO-9, the change in product from 0-D → 3-D → 2-D, i.e., from $(C_4N_2H_{12})UO_2F_4 \cdot 3H_2O$ (UFO-8a) → $(C_4N_2H_{12})U_2O_4F_6$ (MUF-1) → $(C_4N_2H_{12})_2(U_2O_4F_5)_4 \cdot 11H_2O$ (UFO-10), can be understood by examining the local coordination and charge on each uranium. If it is assumed that the major uranium species in solution during the reaction is the $[UO_2F_5]^{3-}$ pentagonal bipyramid, by increasing the $UO_2(CH_3COO)_2 \cdot 2H_2O$ concentration the amount of fluorine bridging of the $[UO_2F_5]^{3-}$ anion should be facilitated. In UFO-8a, each uranium pentagonal bipyramid is a $[UO_{2/1}F_{2/2}F_{3/1}]^{2-}$ anion. That is, each uranium contains a uranyl unit and two bridging and three terminal fluorines. As the concentration of $UO_2(CH_3COO)_2 \cdot 2H_2O$ is increased, the number of terminal fluorines is reduced, subsequently reducing the local charge on each uranium pentagonal bipyramid. For MUF-1, each bipyramid is a $[UO_{2/1}F_{4/2}F_{1/1}]^{-}$ anion, with the number of terminal fluorines reduced from three to one compared with UFO-8a. Increasing the concentration of $UO_2(CH_3COO)_2 \cdot 2H_2O$ further results in the synthesis of UFO-10. In this material, the local coordination and charge on each bypramid is $[UO_{2/1}F_{5/2}]^{0.5-}$. That is, all of the fluorine atoms are now bridging. Thus, there is a *direct relationship* between the $UO_2(CH_3COO)_2 \cdot 2H_2O$ concentration and the local coordination and charge of the uranium pentagonal bipyramids observed in the product phase, i.e., a structural evolution from $[UO_{2/1}F_{2/2}F_{3/1}]^{2-}$ (UFO-8a and -8b), to $[UO_{2/1}F_{4/2}F_{1/1}]^{-}$ (MUF-1), to $[UO_{2/1}F_{5/2}]^{0.5-}$ (UFO-10).

In addition to the changes in the phases observed at a constant $HF_{(aq)}$ concentration, the synthesized product also changes with respect to constant $UO_2(CH_3COO)_2 \cdot 2H_2O$ and piperazine concentrations. On Figure 11, the line marked as **b** represents a constant reagent concentration of $UO_2(CH_3COO)_2 \cdot 2H_2O$; i.e.,

only the piperazine and $HF_{(aq)}$ concentrations are varied. Starting at the piperazine-rich corner and progressing toward the $HF_{(aq)}$ corner, there is a change in synthesized phase from $(C_4N_2H_{12})_2U_2F_{12}{\cdot}H_2O$ (UFO-9), to a mixture of UFO-9, $(C_4N_2H_{12})UO_2F_4{\cdot}3H_2O$ (UFO-8a and -8b), to $(C_4N_2H_{12})U_2O_4F_6$ (MUF-1). With respect to the uranium coordination and local charge, the change is from $[UF_{4/2}F_{4/1}]^{2-}$ (UFO-9) → $[UF_{4/2}F_{4/1}]^{2-} + [UO_{2/1}F_{2/2}F_{3/1}]^{2-}$ (UFO-8a and 8b) → $[UO_{2/1}F_{4/2}F_{1/1}]^{-}$ (MUF-1). At a constant $UO_2(CH_3COO)_2{\cdot}2H_2O$ concentration, increasing the amount of $HF_{(aq)}$ is seen to facilitate greater fluorine bridging of the $[UO_2F_5]^{3-}$ pentagonal bipyramids. However, even at extremely high mole fractions of $HF_{(aq)}$ (0.96), only MUF-1 is observed. At these high $HF_{(aq)}$ mole fractions, the $UO_2(CH_3COO)_2{\cdot}2H_2O$ concentration is too low to completely fluorine bridge the $[UO_2F_5]^{3-}$ moieties, i.e., to produce $(C_4N_2H_{12})_2(U_2O_4F_5)_4{\cdot}11H_2O$ (UFO-10), $[UO_{2/1}F_{5/2}]^{0.5-}$. When the $UO_2(CH_3COO)_2{\cdot}2H_2O$ mole ratio is increased to 0.16, at an $HF_{(aq)}$ fraction of 0.96, we begin to observe the synthesis of UFO-10 as part of a mixture with MUF-1.

The third structural evolution observed occurs at constant piperazine concentrations, i.e., when only the $HF_{(aq)}$ and $UO_2(CH_3COO)_2{\cdot}2H_2O$ concentrations are changed (Figure 11, line **c**). As we progress from the $HF_{(aq)}$-rich corner toward the $UO_2(CH_3COO)_2{\cdot}2H_2O$ corner, the synthesized product changes from pure MUF-1, to a mixture of MUF-1 and UFO-10, to pure UFO-10. With regard to the uranium coordination and local charge, the change is from $[UO_{2/1}F_{4/2}F_{1/1}]^{-}$ (MUF-1) → $[UO_{2/1}F_{4/2}F_{1/1}]^{-} + [UO_{2/1}F_{5/2}]^{0.5-}$ (UFO-10) → $[UO_{2/1}F_{5/2}]^{0.5-}$ (UFO-10). Thus, similar to the trend observed along line **a**, i.e., constant $HF_{(aq)}$ concentration, the increase in the $UO_2(CH_3COO)_2{\cdot}2H_2O$ concentration, and the subsequent decrease of the $HF_{(aq)}$ concentration, results in a greater propensity of fluorine bridging—the fully fluorine-bridged compound, UFO-10, is synthesized.

Similar trends are also observed in the 3g composition space. However, with the additional amount of H_2O, the reduction of $UO_2(CH_3COO)_2{\cdot}2H_2O$ is diminished, as UFO-9 is observed only in a mixture with UFO-8a. In the 5g, 7g, and 9g composition spaces, the reduction of $UO_2(CH_3COO)_2{\cdot}2H_2O$ is not observed, as the molecular phases, UFO-8a and -8b are found in the piperazine-rich corner. In addition, and unlike in the 1g and 3g spaces, UFO-10 is not synthesized, even at high concentrations of $UO_2(CH_3COO)_2{\cdot}2H_2O$, owing to the additional amount of water in the reaction interfering with the complete fluorine bridging of the $[UO_2F_5]^{3-}$ anion.

Physical Properties. Ion-exchange experiments were performed on all of the reported materials except for UFO-8a and -8b, owing to their water solubility. UFO-9 was found to completely exchange Li^+, Na^+, K^+, Rb^+, and Cs^+ as well as Mg^{2+}, Ca^{2+}, Sr^{2+}, and Ba^{2+}, whereas with UFO-10 and MUF-1 only limited exchange (as shown by elemental analysis) was observed with Rb^+ and Cs^+. All of the fully exchanged materials retained crystallinity but not the chain structure seen in UFO-9. They were shown by elemental analyses to contain the exchanged metal as well as an absence of carbon and nitrogen.

The infrared and Raman spectra of the materials revealed broad uranyl stretches for all the U^{VI} materials centered between 890 and 900 cm^{-1} (IR) and between 825 and 850 cm^{-1} (Raman). In addition, U−F bands were observed in all the compounds between 430 and 470 cm^{-1} (IR) and between 420 and 460 cm^{-1} (Raman).

Thermogravimetric measurements on the reported materials indicated the presence (absence) of occluded water with a (no) weight loss occurring between 60 and 110 °C. Water loss calcd (exptl): for $(C_4N_2H_{12})UO_2F_4{\cdot}3H_2O$ (UFO-8a and -8b), 10.63 (10.64); for $(C_4N_2H_{12})_2U_2F_{12}{\cdot}H_2O$ (UFO-9), 4.01 (3.89); for $(C_4N_2H_{12})_2(U_2O_4F_5)_4{\cdot}11H_2O$ (UFO-10), 6.80 (7.43). In addition, all of the materials show a broad weight loss between 250 and 350 °C, consistent with template loss. The resulting calcined material was shown to be U_3O_8 by powder X-ray diffraction.

Conclusion. The systematic investigation of the $UO_2(CH_3COO)_2{\cdot}2H_2O$/HF(aq)/piperazine system has resulted in the synthesis of a variety of compounds whose structures range from molecular, 0-D to framework, 3-D. By utilizing composition space and prism diagrams, we have delineated stability regions wherein pure phase materials can be synthesized. Although a variety of factors are involved in the synthesis of the product phase, one determining factor is the initial $UO_2(CH_3COO)_2{\cdot}2H_2O$ concentration. We observe a direct correlation between the initial concentration of $UO_2(CH_3COO)_2{\cdot}2H_2O$ and the extent of fluorine bridging of the $[UO_2F_5]^{3-}$ moiety in the synthesized phase. That is, we find a synthetic transformation from $(C_4N_2H_{12})UO_2F_4{\cdot}3H_2O$ (UFO-8a and -8b) to $(C_4N_2H_{12})_2(U_2O_4F_5)_4{\cdot}11H_2O$ (UFO-10) or, with respect to the local coordination and charge on the uranium, from $[UO_{2/1}F_{2/2}F_{3/1}]^{2-}$ (UFO-8a and -8b) to $[UO_{2/1}F_{5/2}]^{0.5-}$ (UFO-10). We plan to extend this methodology to other systems and will report on them later.

Acknowledgment. Financial support from the EPSRC is gratefully acknowledged. P.S.H. thanks Christ Church, University of Oxford, for a Junior Research Fellowship.

Supporting Information Available: ORTEP diagrams (50% probability ellipsoids) for UFO-8a, -8b, -9, -10, and MUF-10; powder X-ray diffraction patterns, calculated and observed, for UFO-8a, -8b, -9, -10, and MUF-10; and powder X-ray patterns where phase mixtures were observed for UFO-8a + MUF-1, UFO-8a + UFO-8b, UFO-8b + UFO-9, UFO-10 + MUF-1, UFO-8a + UFO-8b + UFO-9, and UFO-8a + UFO-9 (PDF). A file of X-ray crystallographic data, in CIF format, is also available. This material is available free of charge via the Internet at http://pubs.acs.org.

JA992145F